



Microwave-assisted solution synthesis and photocatalytic activity of Ag nanoparticles supported on ZnO nanostructure flowers

Anukorn Phuruangrat¹ · Nicha Wongwiwat¹ · Titipun Thongtem^{2,3} · Somchai Thongtem^{2,4}

Received: 12 April 2018 / Accepted: 16 August 2018 / Published online: 22 August 2018
© Springer Nature B.V. 2018

Abstract

Ag nanoparticles supported on the surface of three-dimensional (3D) flower-like ZnO nanostructure were synthesized by a microwave-assisted solution method. The obtained products were characterized by X-ray diffraction analysis, field-emission scanning electron microscopy, Fourier-transform infrared spectroscopy, Raman spectrophotometry, X-ray photoelectron spectroscopy, and photoluminescence spectroscopy. The analytical results confirmed homogeneously distributed Ag nanoparticles supported on the surface of flower-like ZnO nanostructure. The photocatalytic effect of the heterostructure Ag/ZnO nanocomposites was investigated using photodegradation under ultraviolet (UV) light of methylene blue as model dye. The heterostructure Ag/ZnO nanocomposites exhibited much higher photocatalytic activity than pure ZnO flowers. The improved photocatalytic properties are attributed to formation of a Schottky barrier at the metal–semiconductor interface of the Ag/ZnO nanocomposites.

Keywords Ag/ZnO nanocomposites · Spectroscopy · Photocatalysis

✉ Anukorn Phuruangrat
phuruangrat@hotmail.com

✉ Somchai Thongtem
schthongtem@yahoo.com

¹ Department of Materials Science and Technology, Faculty of Science, Prince of Songkla University, Hat Yai, Songkhla 90112, Thailand

² Materials Science Research Center, Faculty of Science, Chiang Mai University, Chiang Mai 50200, Thailand

³ Department of Chemistry, Faculty of Science, Chiang Mai University, Chiang Mai 50200, Thailand

⁴ Department of Physics and Materials Science, Faculty of Science, Chiang Mai University, Chiang Mai 50200, Thailand

Introduction

Air and water pollution currently represent some of the most crucial problems on Earth. Due to its simple decomposition process, photocatalysis has become an efficient approach for degradation of organic and toxic pollutants in water and air [1–4]. Zinc oxide (ZnO) with a direct bandgap of 3.37 eV at room temperature, large excitonic binding energy of 60 meV, and Hall mobility on the order of $200 \text{ cm}^2 \text{ V}^{-1} \text{ s}^{-1}$ at room temperature is one of the most attractive materials among the group II–VI semiconductors. It has a wide variety of applications in electronic and optoelectronic devices such as catalysis, gas sensors, piezoelectric devices, dye-sensitized solar cells, and photochemical degradation of organic pollutants [5–10]. However, the photocatalytic activity of ZnO is limited by recombination of photogenerated electrons and holes, which reduces its photocatalytic efficiency [7, 8, 11, 12]. Several methods have been applied to improve the photocatalytic properties of metal oxides, including metal doping [5, 13, 14], formation of heterostructures with semiconductors [10, 12], and deposition of noble metals [7, 9, 15]. Among these, loading with noble metals has been considered to be the most efficient strategy for improving the photocatalytic properties of ZnO [7, 8, 15, 16]. Introduction of interfaces between ZnO and noble metals such as Pt [7, 9, 15], Ag [8, 16], and Au [17, 18] can improve the photocatalytic activity of ZnO, because photoinduced charges diffuse across the junction between the noble metal and ZnO and the recombination process is reduced [16]. Among noble metals, Ag is very attractive because of its low cost, nontoxicity, and high electrical and thermal conductivity [8].

In the work presented herein, Ag nanoparticles supported on 3D flower-like ZnO nanostructure were synthesized using a microwave-assisted solution method, and their photocatalytic performance investigated using photodegradation under UV radiation of methylene blue as model dye.

Experimental

Flower-like ZnO samples were prepared using a direct precipitation method. First, 13.3866 g $\text{Zn}(\text{NO}_3)_2 \cdot 6\text{H}_2\text{O}$ was dissolved in 200 ml reverse-osmosis (RO) water under continuous stirring. Subsequently, 40 ml 3 M NaOH solution was added to the Zn^{2+} solution under vigorous stirring for 24 h to form white precipitate, which was filtered, washed, and dried. Finally, the precipitate was calcined at $600 \text{ }^\circ\text{C}$ with heating rate of $5 \text{ }^\circ\text{C min}^{-1}$ for 2 h in ambient atmosphere.

To prepare Ag/ZnO nanocomposites, AgNO_3 with 1 wt%, 5 wt%, and 10 wt% Ag was dissolved in 100 ml ethylene glycol containing 2.5 g ZnO suspension under constant stirring for 30 min, then heated in a 300-W microwave oven for 10 min. The as-prepared precipitates were collected, washed with deionized water, and dried for further characterization.

The crystallinity and crystalline phase of the as-prepared nanostructure were analyzed using an X-ray diffractometer (Philips X'Pert MPD XRD) with Cu K_α radiation in the range of 20° to 70° . Morphology investigation was carried out by

field-emission scanning electron microscopy (JEOL JSM 6335F FE-SEM). Fourier-transform infrared (Perkin Elmer Spectrum RX FTIR) spectrometry was carried out at room temperature in the range of 400 cm^{-1} to 4000 cm^{-1} on pellets prepared by 40 times KBr dilution. Raman spectrophotometry (T64000 HORIBA Jobin-Yvon) was carried out at 50 mW using a green Ar laser at wavelength of 514.5 nm. X-ray photoelectron spectrophotometry (XPS) was carried out using an Axis Ultra DLD (Kratos Analytical Ltd.) with a monochromated Al K_{α} (1486.6 eV) source. All XPS spectra were calibrated to the C 1s electron peak at 285.1 eV. Photoemission was characterized by photoluminescence (PL) spectroscopy (PerkinElmer LS 50B) at room temperature.

Methylene blue (MB) was used as probe molecule to evaluate photocatalytic activity. Photocatalysis was conducted using 200 mg catalyst dispersed in 200 ml 1×10^{-5} M MB aqueous solution under UV light at room temperature. Prior to irradiation, the suspension was magnetically stirred in the dark for 30 min to establish adsorption–desorption equilibrium of methylene blue on the photocatalytic surface. During testing, approximately 5 ml solution was withdrawn every 10 min. Before analysis for MB content, the aqueous solutions were centrifuged to remove any suspended solid catalyst particles. The residual content of methylene blue was measured at 664 nm using a UV–Vis spectrophotometer (PerkinElmer Lambda 25) with deionized water as reference. The decolorization percent was calculated as

$$\text{Decolorization efficiency(\%)} = \frac{C_0 - C}{C_0} \times 100, \quad (1)$$

where C_0 is the initial dye concentration and C is the dye concentration after photocatalytic treatment.

Results and discussion

Figure 1 shows the XRD patterns of the pure ZnO sample and as-prepared heterostructure Ag/ZnO nanocomposites. It can be seen that the pure sample could be indexed to the pure phase of hexagonal wurtzite ZnO structure in Joint Committee on Powder Diffraction Standard (JCPDS) card no. 36-1451 [19]. The diffraction peaks at 2θ of 31.79° , 34.42° , 36.25° , 47.51° , 56.62° , 63.17° , 66.08° , 68.30° , and 69.41° correspond to (100), (002), (101), (102), (110), (103), (200), (112), and (201) planes of hexagonal wurtzite ZnO structure, respectively. In comparison, the XRD patterns of the Ag/ZnO nanocomposites with different Ag loading contents included a major phase of wurtzite ZnO with additional peaks at 2θ of 38.2° , 44.5° , and 64.6° , corresponding to (111), (200), and (220) planes of face-centered-cubic metallic Ag as minor phase in JCPDS card no. 04-0783 [19].

The XPS spectra of the 10 wt% Ag/ZnO nanocomposite (Fig. 2) were calibrated using the C 1s peak at 285.1 eV. The XPS survey scan revealed presence of binding energies of the main constituents of the 10 wt% Ag/ZnO nanocomposite. The XPS spectra confirmed presence of Zn, O, and Ag in the 10 wt% Ag/ZnO nanocomposite. The high-resolution Ag 3d XPS spectrum showed two peaks centered at 367.2 and 373.2 eV, corresponding to Ag $3d_{5/2}$ and Ag $3d_{3/2}$ [8, 20]. The Ag

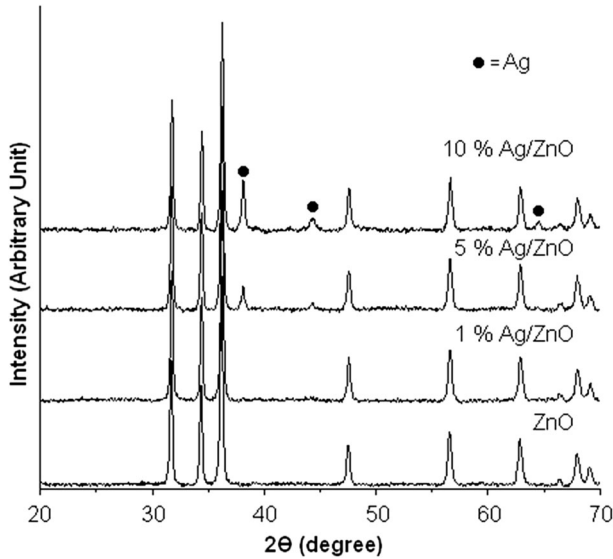


Fig. 1 XRD patterns of pure ZnO sample prepared by direct precipitation method and 1, 5, and 10 wt% Ag/ZnO nanocomposites prepared by microwave-assisted solution method

3d region showed well-separated spin-orbit components of 6.0 eV, corresponding to the characteristic peaks of metallic Ag, which indicates presence of Ag^0 - nanoparticles [8, 20]. The high-resolution XPS spectrum of the Zn 2p region showed Zn 2p_{3/2} and Zn 2p_{1/2} peaks at around 1021.70 eV and 1044.80 eV, with spin-orbit splitting of 23.10 eV, confirming presence of Zn^{2+} of the ZnO crystal lattice [7, 8, 17, 18]. The O 1s XPS peak was detected at 531.28 eV, being attributed to O^{2-} ions in the ZnO lattice [7, 8, 17, 18].

Figure 3a shows the Raman spectra of the 0, 1, 5, and 10 wt% Ag/ZnO samples characterized using the green Ar-ion laser with excitation at wavelength of 514.5 nm, in the wavenumber range of 200 cm^{-1} to 800 cm^{-1} . A_1 and E_1 are polar in nature and split into transverse optical (TO) and longitudinal optical (LO) modes. The E_2 mode consists of low (E_2 low) and high (E_2 high) frequency phonons, associated with Zn and O atomic vibration [21, 22]. The Raman spectrum of pure ZnO showed a dominant peak at 437 cm^{-1} , which corresponds to the E_2 mode characteristic of the wurtzite ZnO structure [6, 21, 22]. Other weak Raman peaks at 331, 381, and 583 cm^{-1} were assigned to $E_2(\text{high})$ - $E_2(\text{low})$, $A_1(\text{TO})$, and $E_1(\text{LO})$ modes, respectively. The $E_1(\text{LO})$ mode is commonly related to various defects such as oxygen vacancies, Zn interstitials, and defect complexes [6, 21, 22]. The Raman spectrum of the 10 wt% Ag/ZnO nanocomposite showed a low-intensity E_2 mode introduced by local strain in the host ZnO lattice around the Ag-ZnO interface. A broad peak at 563 cm^{-1} of the silent B_1 (low) mode is related to the change in lattice strain, consequently leading to disorder lattice [23]. Thus, the silent mode observed for the 10 wt% Ag/ZnO nanocomposite indicates a greater extent of Ag attachment and higher degree of disorder.

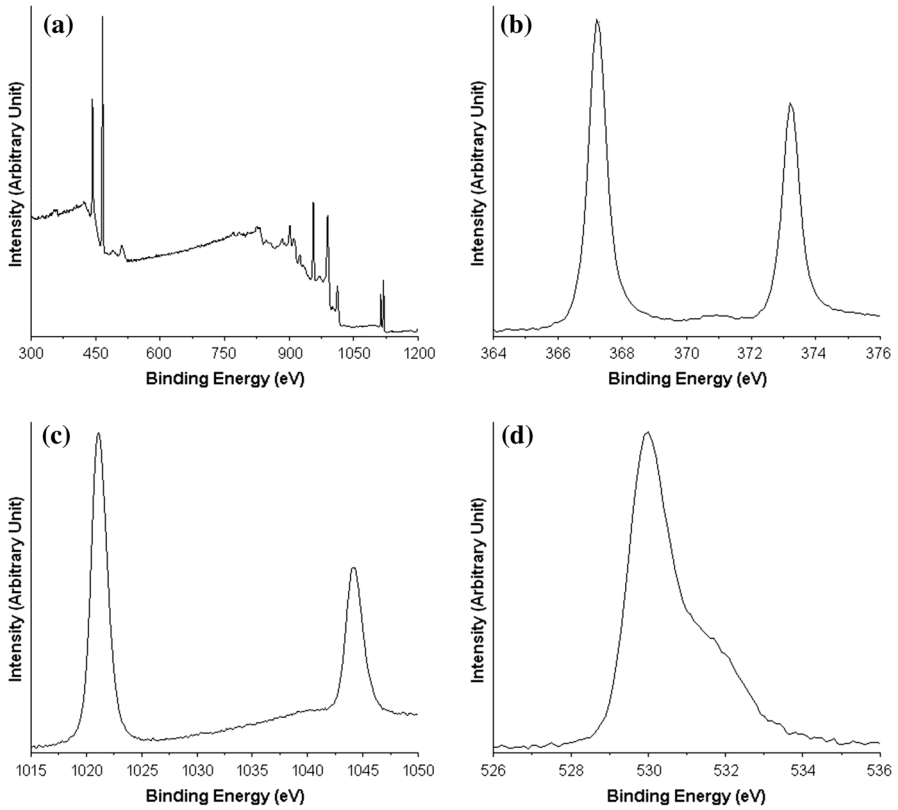


Fig. 2 a XPS survey spectrum, and high-resolution spectra of **b** Ag 3d, **c** Zn 2p, and **d** O 1s of 10 wt% Ag/ZnO nanocomposite

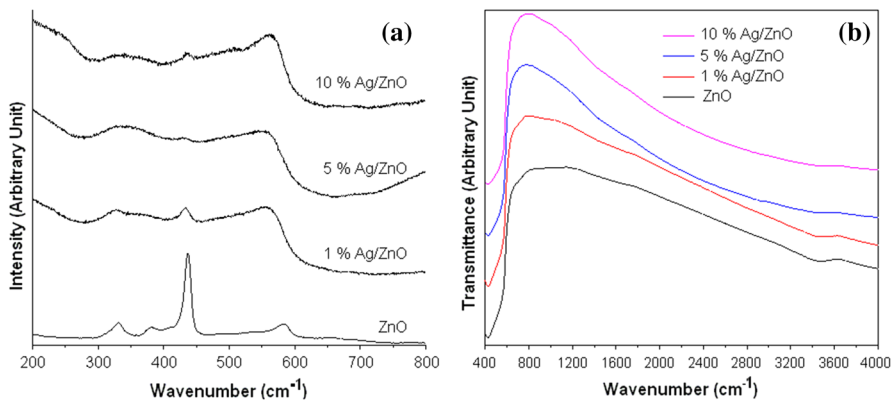


Fig. 3 a Raman and **b** FTIR spectra of pure ZnO sample prepared by direct precipitation method and 1, 5, and 10 wt% Ag/ZnO nanocomposites prepared by microwave-assisted solution method

Figure 3b shows the FTIR spectra of the ZnO and Ag/ZnO samples. The transmittance detected at 425 cm^{-1} was assigned to the stretching mode of Zn–O bond [5, 21]. The band at 3424 cm^{-1} is related to stretching of O–H group, indicating presence of surface-adsorbed water molecules or hydroxyl groups on the samples [5, 21].

Figures 4 and 5a show SEM images of the pure ZnO sample and heterostructure Ag/ZnO nanocomposites with different Ag loadings. The result for the pure ZnO sample clearly reveals the uniform flower-shaped ZnO structure composed of nanoplate clusters with large voids. SEM images of 5 wt% and 10 wt% Ag/ZnO nanocomposites revealed homogeneous distribution of Ag nanoparticles supported on the surface of flower-like ZnO structure. The high-magnification SEM image of the 10 wt% Ag/ZnO nanocomposite revealed Ag nanoparticles with size less than 100 nm, supported on the surface of ZnO petals, which could improve the photocatalytic activity of ZnO by formation of a Schottky barrier or a potential barrier for electrons formed at the metallic Ag–ZnO semiconductor interface [8, 17]. The chemical composition was obtained by EDS analysis. EDS mapping of the 10 wt% Ag/ZnO nanocomposite (Fig. 5b–d) revealed only Ag, Zn, and O elements. Obviously, Ag metal was highly distributed on the surface of ZnO. The atomic percent of the elements was revealed to be 45.89, 45.31, and 8.80 % for Zn, O, and Ag, respectively, for the 10 wt% Ag/ZnO nanocomposite. All these results can be basically related to metallic Ag adsorbed on the ZnO surface.

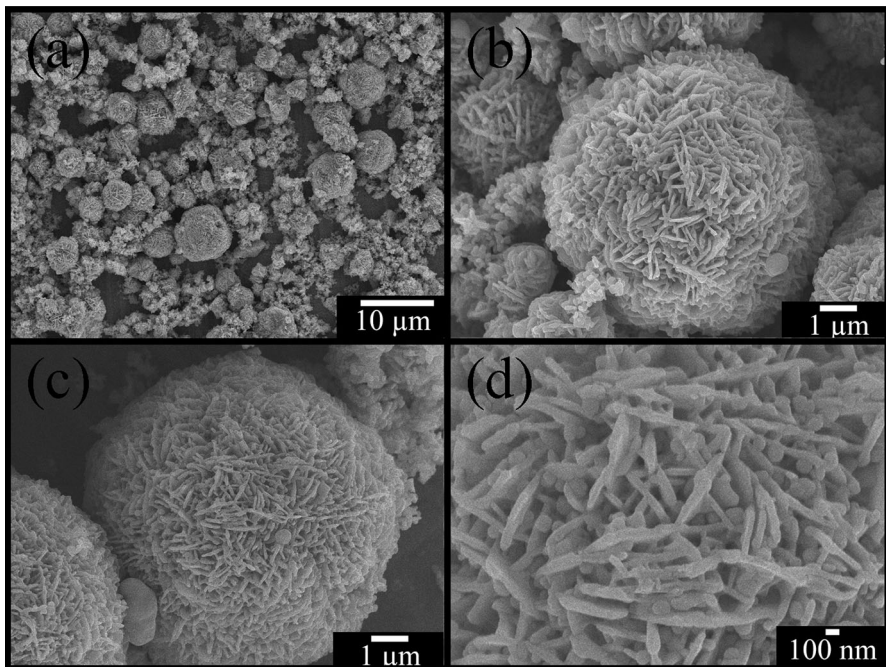


Fig. 4 SEM images of **a** ZnO, **b** 5 wt% Ag/ZnO, and **c**, **d** 10 wt% Ag/ZnO samples

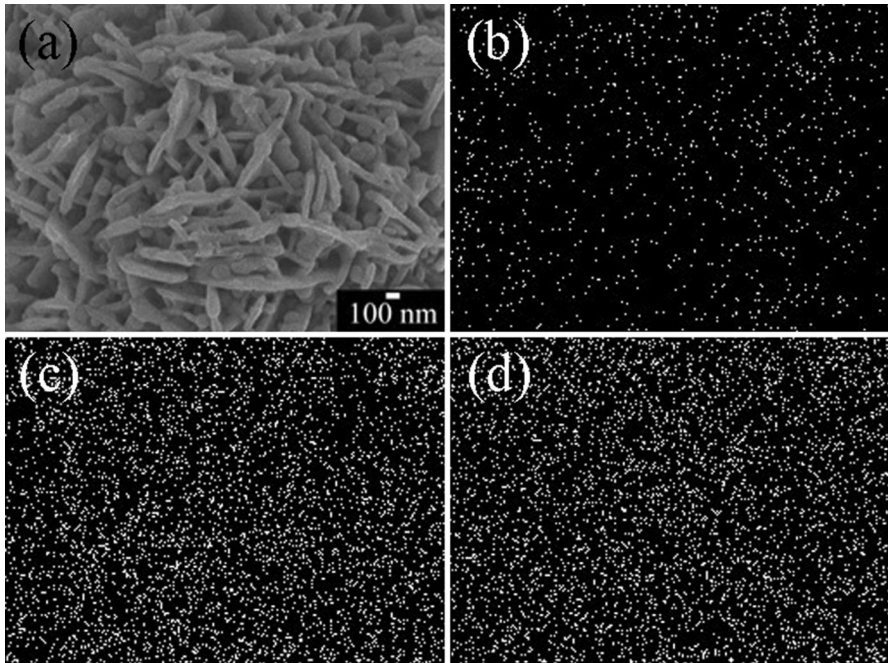
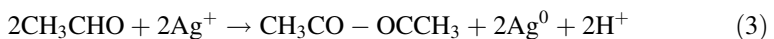


Fig. 5 a SEM image, and EDS mapping of b Ag, c Zn, and d O of 10 wt% Ag/ZnO nanocomposite prepared by microwave-assisted solution method

To form the Ag/ZnO nanocomposites, ethylene glycol was used as reducing reagent to reduce Ag^+ to Ag^0 with microwave induction. The metallic nanoparticles formed as follows:



The Ag^+ ions were adsorbed on the surface of the flower-like ZnO nanostructure. Under microwave irradiation, Ag^+ ions were reduced. Ag^0 nucleated and grew to form nanoparticles on the surface of ZnO flowers [24–26].

Figure 6a shows the photocatalytic efficiency for degradation of MB solution by the pure ZnO and different Ag/ZnO nanocomposites induced by UV radiation. In this research, the photocatalytic efficiency of pure ZnO flowers for photodegradation of MB was almost 42 %. The photocatalytic efficiency was greatly improved by surface modification of the ZnO petals. Obviously, the photocatalytic activity of the Ag/ZnO nanocomposites was related to the Ag content loaded on the ZnO petals. For 10 wt% Ag, the efficiency of the MB degradation increased to almost 96 % under UV radiation within 300 min. Figure 6b shows the reaction kinetics for the pure ZnO sample and Ag/ZnO nanocomposites fit using Langmuir–Hinshelwood kinetics [21, 27],

$$\ln(C_0/C_t) = kt, \quad (4)$$

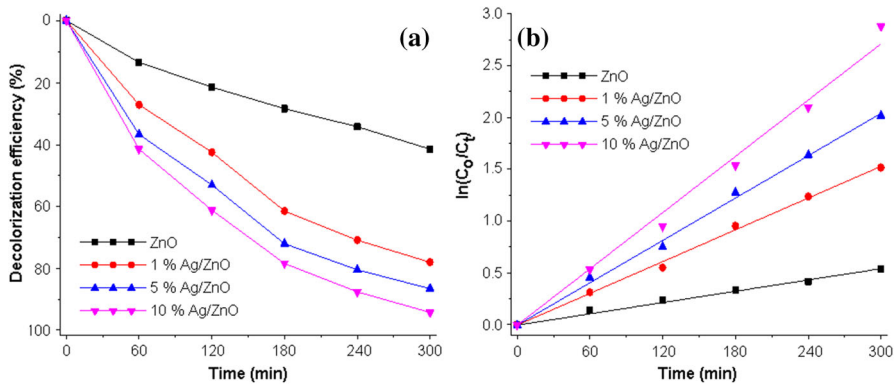


Fig. 6 **a** Decolorization efficiency and **b** first-order plot for photocatalytic degradation of MB by ZnO flowers with different Ag contents induced by UV radiation

where k is the pseudo-first-order rate constant for time period t . All the reactions were found to obey pseudo-first-order kinetics, as confirmed by the slopes of the reaction profiles [3, 8, 16, 22]. The rate constant fit well with the pseudo-first-order reaction kinetics. The highest rate constant was $9.11 \times 10^{-3} \text{ min}^{-1}$, and the half-life ($t_{1/2}$) was 76.09 min for the 10 wt% Ag/ZnO nanocomposite. The rate constant and half-life were $1.80 \times 10^{-3} \text{ min}^{-1}$ and 385.08 min for ZnO, $5.05 \times 10^{-3} \text{ min}^{-1}$ and 137.26 min for 1 wt% Ag/ZnO, and $6.73 \times 10^{-3} \text{ min}^{-1}$ and 102.99 min for 5 wt% Ag/ZnO, within 300 min. These results clearly demonstrated that the 10 wt% Ag/ZnO nanocomposite showed the highest photocatalytic degradation of MB dye solution under UV radiation. This enhancement can be ascribed to formation of a Schottky barrier and the surface plasmon resonance (SPR) or the resonant vibration of photogenerated diffusion electrons at the junction between the n - and p -type materials of the Ag/ZnO nanocomposites induced by incident UV [16, 20, 27]. The photogenerated electrons diffused from the ZnO conduction band (CB) to the Fermi level of Ag, leading to strongly stabilized photogenerated holes in the valence band (VB) of ZnO [16, 20], in accordance with the PL properties, as shown by the results in Fig. 7. It can be seen that the PL intensity of the 10 wt% Ag/ZnO nanocomposite was lower than that of the pure ZnO sample, due to the decreased recombination rate of electrons and holes in the 10 wt% Ag/ZnO nanocomposite. Ag nanoparticles on ZnO can act as traps for photogenerated electrons [28–30]. When the ZnO nanopetals and Ag nanoparticles are in direct contact with each other, electrons will diffuse from energy levels of ZnO to those of Ag. Thus, Ag nanoparticles on the surface of ZnO help prolong the lifetime of photogenerated electron–hole pairs in ZnO [20].

Under UV–visible irradiation, photons with energy greater than the bandgap of ZnO can excite electrons from the valence to conduction band. The positive holes oxidize OH^- to form $\cdot\text{OH}$ radicals, while the electrons in the CB are rapidly trapped by molecular oxygen to form superoxide radical anions [16, 17, 21]. Both radicals contribute to degrade pollutant molecules. Modification of ZnO by Ag nanoparticles effectively enhanced its photocatalytic activity due to formation of a Schottky

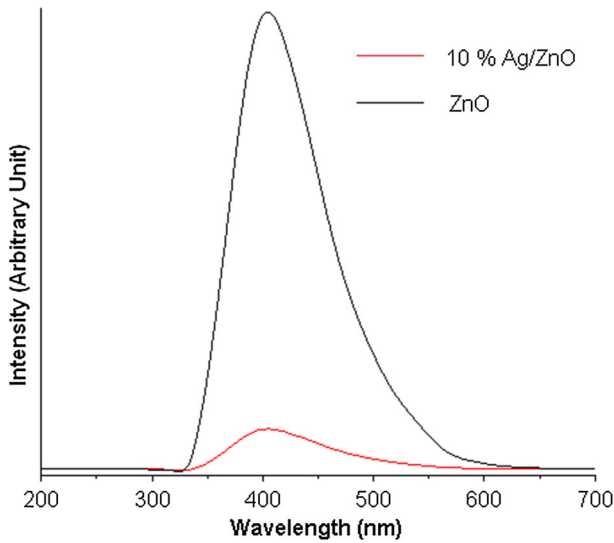


Fig. 7 PL spectra of ZnO and 10 wt% Ag/ZnO photocatalysts

barrier at the metal–semiconductor junction, as shown by the results in Fig. 8 [8, 17]. The new Fermi level of the Ag/ZnO nanocomposites was lower. Thus, photogenerated electrons could diffuse from the CB of ZnO to the Ag nanoparticles, driven by the above potential energy. Subsequently, the electrons were trapped by O_2 and H_2O to form $\cdot OH$ radicals while holes were trapped by OH^- to form $\cdot OH$ radicals [27, 31]. These radicals act as strong oxidizing agents that can decompose the organic dye to H_2O and CO_2 as final products. Thus, the Ag nanoparticles play an important role in separation of photogenerated electrons and holes to improve the photocatalytic activity.

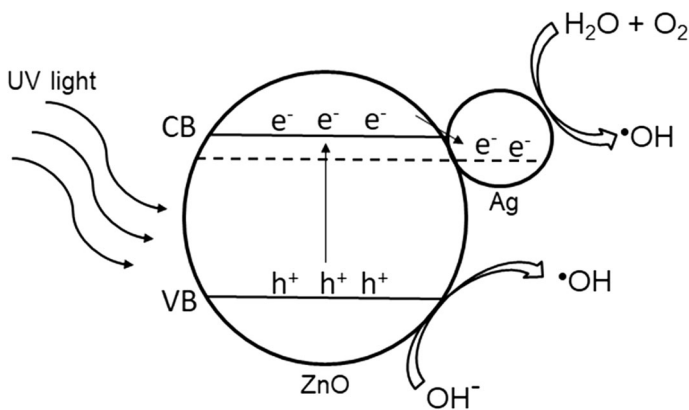


Fig. 8 Schematic diagram for photocatalysis of Ag/ZnO nanocomposites

Conclusions

Ag nanoparticles supported on the surface of 3D ZnO heterostructure flowers were successfully synthesized using a microwave-assisted solution method. Photodegradation of MB by the heterostructure Ag/ZnO nanocomposites was more efficient than that by the pure ZnO sample. Enhanced photocatalytic efficiency for photodegradation of MB was observed for Ag nanoparticles supported on the surface of ZnO flowers. The 10 wt% Ag/ZnO nanocomposite exhibited almost 100 % photodegradation within 300 min induced by UV radiation.

Acknowledgements The authors thank Prince of Songkla University, Hat Yai, Songkhla 90112, Thailand for financial support under contact SCI1610775S.

References

1. S. Yao, F. Qu, G. Wang, X. Wu, *J. Alloys Compd.* **724**, 695 (2017)
2. A. Tuerdi, A. Abdukayum, P. Chen, *Mater. Lett.* **209**, 235 (2017)
3. B. Song, Q. Tang, Q. Li, W. Wu, H.L. Zhang, J. Cao, M. Ma, *Mater. Lett.* **209**, 251 (2017)
4. X. Ren, H. Fan, J. Ma, C. Wang, M. Zhang, N. Zhao, *Appl. Surf. Sci.* **441**, 194 (2018)
5. V. Etacheri, R. Roshan, V. Kumar, A.C.S. *Appl. Mater. Interfaces* **4**, 2717 (2012)
6. Y. Wang, X. Li, G. Lu, X. Quan, G. Chen, *J. Phys. Chem. C* **112**, 7332 (2008)
7. S. Li, K. Zhang, J. Wang, B. Yan, C. Wang, Z. Xiong, H. Xu, Y. Du, *Sensor. Actuat. B* **252**, 717 (2017)
8. H. Mou, C. Song, Y. Zhou, B. Zhang, D. Wang, *Appl. Catal. B* **221**, 565 (2018)
9. H. Tian, H. Fan, J. Ma, Z. Liu, L. Ma, S. Lei, J. Fang, C. Long, *J. Hazard. Mater.* **341**, 102 (2018)
10. H. Tian, H. Fan, J. Ma, L. Ma, G. Dong, *Electrochim. Acta* **247**, 787 (2017)
11. L. Ma, H. Fan, K. Fu, S. Lei, Q. Hu, H. Huang, G. He, *ACS Sust. Chem. Eng.* **5**, 7093 (2017)
12. C. Wang, H. Fan, X. Ren, J. Fang, *Appl. Phys. A* **124**, 99 (2018)
13. O. Yayapao, T. Thongtem, A. Phuruangrat, S. Thongtem, *Mater. Lett.* **90**, 83 (2013)
14. A. Phuruangrat, O. Yayapao, T. Thongtem, S. Thongtem, *Superlatt. Microstr.* **67**, 118 (2014)
15. W. Zhang, G. Wang, Z. He, C. Hou, Q. Zhang, H. Wang, Y. Li, *Mater. Des.* **429**, 109 (2016)
16. R. Pagano, A. Quarta, S. Pal, A. Licciulli, L. Valli, S. Bettini, *J. Phys. Chem. C* **121**, 27199 (2017)
17. J. Lu, H. Wang, D. Peng, T. Chen, S. Dong, Y. Chang, *Physica E* **78**, 41 (2016)
18. A. Senthilraja, B. Krishnakumar, B. Subash, Abilio J.F.N. Sobral, M. Swaminathan, M. Shanthi, *J. Ind. Eng. Chem.* **33**, 51 (2016)
19. Powder Diffract. File, JCPDS-ICDD, 12 Campus Bld., Newtown Square, PA 19073–3273, USA (2001)
20. J. Lv, Q. Zhu, Z. Zen, M. Zhang, J. Yang, M. Zhao, W. Wang, Y. Cheng, G. He, Z. Sun, *J. Phys. Chem. Solids* **111**, 104 (2017)
21. A. Phuruangrat, S. Thongtem, T. Thongtem, *Mater. Des.* **107**, 250 (2016)
22. O. Yayapao, T. Thongtem, A. Phuruangrat, S. Thongtem, *Mater. Sci. Semicond. Process.* **39**, 786 (2015)
23. N. Gogurla, S. Bayan, P. Chakrabarty, S.K. Ray, *J. Lumin.* **194**, 15 (2018)
24. Q.Q. Xu, Y.L. Ma, G. Xu, J.Z. Yin, A.Q. Wang, J.J. Gao, *J. Supercrit. Fluid.* **92**, 100 (2014)
25. J.J. Zhu, C.X. Kan, J.G. Wan, M. Han, G.H. Wang, *J. Nanomater.* 2011, 1, Art. ID 982547 (2011)
26. J. Zhu, C. Kan, Y. Wu, J. Wan, M. Han, G. Wang, *J. Nanomater.* 2016, 1, Art. ID 5812739 (2016)
27. H. Liu, Y. Hu, Z. Zhang, X. Liu, H. Jia, B. Xu, *Appl. Surf. Sci.* **355**, 644 (2015)
28. B. Sarm, S.K. De, B.K. Sarm, *J. Phys. Conf. Ser.* 765, 1, Art. ID 012023 (2016)
29. H. Liu, Y. Hu, X. He, H. Jia, X. Liu, B. Xu, *J. Alloys Compd.* **650**, 633 (2015)
30. H. Liu, H. Zhai, C. Hu, J. Yang, Z. Liu, *Nanoscale Res. Lett.* **12**, 466 (2017)
31. H. Wang, X. Liu, S. Han, *CrystEngComm* **18**, 1933 (2016)